Evoked potentials as a biomarker of remyelination

Moones Heidari[a,1], Abigail B. Radcliff[a,1], Gillian J. McLellan[b,c], James N. Ver Hoeve[b], Kore Chan[c], Julie A. Kiland[b], Nicholas S. Keuler[d], Benjamin K. August[e], Dylan Sebo[a], Aaron S. Field[f], and Ian D. Duncan[a,2]

[a]Department of Medical Sciences, School of Veterinary Medicine, University of Wisconsin–Madison, Madison, WI 53706; [b]Department of Ophthalmology and Visual Sciences, School of Medicine and Public Health, University of Wisconsin–Madison, Madison, WI 53705; [c]Department of Surgical Sciences, School of Veterinary Medicine, University of Wisconsin–Madison, Madison, WI 53706; [d]Department of Statistics, College of Letters and Science, University of Wisconsin–Madison, Madison, WI 53706; [e]Electron Microscope Facility, School of Medicine and Public Health, University of Wisconsin–Madison, Madison, WI 53706; and [f]Department of Radiology, School of Medicine and Public Health, University of Wisconsin–Madison, Madison, WI 53792

Edited by Lawrence Steinman, Stanford University School of Medicine, Stanford, CA, and approved November 18, 2019 (received for review April 12, 2019)

Multiple sclerosis (MS) is a common cause of neurologic disease in young adults that is primarily treated with disease-modifying therapies which target the immune and inflammatory responses. Promotion of remyelination has opened a new therapeutic avenue, but how best to determine efficacy of remyelinating drugs remains unresolved. Although prolongation and then shortening of visual evoked potential (VEP) latencies in optic neuritis in MS may identify demyelination and remyelination, this has not been directly confirmed. We recorded VEPs in a model in which there is complete demyelination of the optic nerve, with subsequent remyelination. We examined the optic nerves microscopically during active disease and recovery, and quantitated both demyelination and remyelination along the length of the nerves. Latencies of the main positive component of the control VEP demonstrated around 2-fold prolongation during active disease. VEP waveforms were nonrecordable in a few subjects or exhibited a broadened profile which precluded peak identification. As animals recovered neurologically, the VEP latencies decreased in association with complete remyelination of the optic nerve but remained prolonged relative to controls. Thus, it has been directly confirmed that VEP latencies reflect the myelin status of the optic nerve and will provide a surrogate marker in future remyelination clinical trials.

demyelination | remyelination | optic nerve | VEP | animal model

Remyelination in multiple sclerosis (MS) is a major therapeutic target as it will restore conduction in demyelinated axons and protect them against ongoing degeneration (1). It has been thoroughly documented that remyelination of demyelinated axons in the spinal cord by oligodendrocytes (2, 3) results in significant recovery of nerve conduction velocities. Remyelination has been unequivocally shown to restore normal neurologic function after both focal (4) and global demyelination (5), likely through the recovery of nerve conduction.

Optic neuritis is a frequent and often initial symptom in MS, resulting in variable visual disturbance (6, 7). Visual evoked potentials (VEPs) have been extensively used to monitor the disease course during optic neuritis and in early and late recovery (6, 8–11). In acute disease, the amplitude of the VEP is usually decreased, likely resulting from inflammation, edema, demyelination, and some axon loss (9). Thereafter, the latency of the VEP increases, probably resulting from demyelination, but in patients followed long term, the latency can decrease, an outcome that has been suggested, although not proved, to result from remyelination (8, 9). In unilateral optic neuritis, abnormal VEPs with increased latency have been frequently identified in the clinically unaffected eye (12, 13). Also, latency delays can be found in patients with MS with no history of optic neuritis (14). While remyelination may be the primary reason for partial recovery of the VEP latency, it is possible that central nervous system (CNS) plasticity may account for the recovery due to redistribution of ion channels in demyelinated axons (15).

However, the pathological changes in the optic nerves (ONs) of patients with MS who have been rigorously evaluated using VEPs during acute disease and recovery have not been studied. Indeed, there have been very few neuropathological studies of the ONs in patients with MS (16, 17). Thus, the interpretation of the myelin changes in the ON underpinning delayed latencies and decrease in amplitude of VEPs has largely relied on extrapolation from data on demyelination/remyelination of the spinal cord in animal models (2, 18). Generating similar demyelinating lesions in the ON has relied predominantly on the injection of either lysolecithin or antigalactocerebroside antiserum directly into the rat (19, 20), cat (21, 22), or nonhuman primate ON (23) or into the optic chiasm (20). Using this approach, it has been shown that prolongation of the VEP latency depends on lesion size, but the effect of remyelination on latency has not been shown experimentally. However, the creation of ON lesions is fraught with technical challenges, and thus a more robust and reproducible model would be advantageous. Cuprizone toxicity, the de facto model of demyelination and remyelination, does not result in ON demyelination and experimental autoimmune encephalitis (EAE) is inconsistent in its effects on the ON and hence is an unreliable model in which to study remyelination (24). Thus, to date there has been a lack of models with reproducible optic neuropathy and lesions limited to demyelination and then remyelination that can be used to evaluate the myelin status by VEPs.

This is a critical need in the development of definitive outcome measures in MS clinical trials of remyelination (25–31). Recently, 2 clinical trials in MS, testing the remyelination-promoting effect of 2 drugs, the first one a monoclonal antibody, opicinumab

Significance

Remyelination is a critical therapeutic target in MS that will restore function and protect demyelinated axons. Clinical trials of putative remyelination-promoting drugs depend on valid, robust, and noninvasive outcome measures. To date, MRI has failed to provide outcome metrics sufficiently sensitive and specific to remyelination. Optic neuritis is a common symptom of MS and visual evoked potentials (VEPs) have been proposed to identify demyelination during acute disease and subsequent remyelination, but this is unproven. Here, we use an animal model with severe optic nerve demyelination and subsequent remyelination to show that the VEP latency truly measures these myelin sheath changes. Hence, the VEP can be used as an outcome measure in future MS trials in which remyelination is the goal.

Author contributions: M.H., J.N.V.H., and I.D.D. designed research; M.H., A.B.R., J.A.K., B.K.A., and I.D.D. performed research; M.H., A.B.R., G.J.M., J.N.V.H., K.C., N.S.K., D.S., and I.D.D. analyzed data; and M.H., A.B.R., G.J.M., J.N.V.H., A.S.F., and I.D.D. wrote the paper.

The authors declare no competing interest.

This article is a PNAS Direct Submission.

[1]M.H. and A.B.R. contributed equally to this work.

[2]To whom correspondence may be addressed. Email: ian.duncan@wisc.edu.

This article contains supporting information online at https://www.pnas.org/lookup/suppl/doi:10.1073/pnas.1906358116/-/DCSupplemental.

First published December 16, 2019.

(anti-LINGO1) (32), and the second one the antimuscarinic drug, clemastine fumarate (33), used the VEP as the main outcome measure. The latter trial showed subtle decreases in the VEP latency in treated patients (33), but these effects were modest and in both trials, definitive evidence of the therapeutic enhancement of remyelination was indirect.

To address this question, we have used a large-animal model of demyelination–remyelination in the feline called feline irradiated diet-induced demyelination (FIDID) (5) that results from being fed irradiated food (5, 34–36). Global demyelination of the CNS results in the development of marked neurologic disease followed by neurologic recovery on return to nonirradiated food. We therefore used this model to determine whether VEP latency and amplitude corresponded to pathologic changes in the ON and whether slowing of VEP latencies resulted from pure demyelination. Subsequently, on recovery, we tested whether remyelination resulted in shortening of VEP latency. These VEP data were compared to the extent of remyelination, which was mapped and quantitated along the length of the ONs. To exclude the possibility of confounding effects of retinal involvement on the VEP, we also carried out electroretinography and optical coherence tomography.

Results

Clinical Course. Sixteen cats were followed from the time of onset of neurologic disease that was progressive over 3 to 4 wk. In 5 cats, neurologic abnormalities began after 6 mo of consuming the irradiated diet as previously reported (5). These clinical signs arose from the generalized demyelination of the CNS. We therefore used the clinical neurologic score (*Materials and Methods*) as a surrogate marker of ongoing demyelination and remyelination in the ON. Despite the almost total myelin loss in the nerve, vision was remarkably unaffected except in one cat that became clinically blind and another in which vision appeared reduced. VEPs were recorded before the development of neurologic disease and at times thereafter as they became affected (neurologic score + to +++) and recovered (+++ to + or 0) (Fig. 1). In 11 cats, the neurologic disease developed late and was more protracted and the VEP recordings are reported from the time at which progressive neurologic disease was first identified.

VEPs. The control feline flash VEP recorded from the scalp overlying the occipital cortices was characterized by a variable complex of short-latency (peak time ≤35 ms) positive and negative wavelets that immediately preceded a major positive peak (P2). As the short-latency complex is highly variable between individual cats, amplitude and latencies of its component wavelets were not analyzed in the present study (37). During active disease when cats exhibited clinically appreciable neurologic deficits, VEP latency (peak time) of P2 was significantly prolonged relative to control values (active disease latency mean [SD] = 98.88 [14.76] ms, n = 15 animals; control latency = 58.46 [9.11] ms, n = 25 animals; $P <$ 0.0001). Clinical neurologic improvement on return to feeding a nonirradiated diet was associated with subsequent shortening of the latency of the VEP P2 component relative to active disease values (after recovery latency = 76.28 [9.85] ms, n = 6 animals, P = 0.0005), but remained significantly different from control values (P = 0.0035) (Fig. 2 *A*, *C*, and *E*). The VEP latency changes for each recovered animal are also shown in *SI Appendix*, Table S2, along with g-ratio measurements in 3 of the recovered cats.

In contrast to latency values, VEP amplitude showed pronounced interindividual variability within all groups but was relatively unaffected in FIDID (Fig. 2 *A* and *F*). Varying degrees of lateral asymmetry of these occipital VEP amplitudes were frequently encountered in all groups and attributable to asymmetric decussation and projection of ON fibers at the chiasm in this species, in which an estimated 25% to 40% of retinal nerve fibers project to the ipsilateral cerebral hemisphere (38). Although mean amplitude was significantly higher in recovered cats with ON remyelination than in the control reference population (after recovery amplitude = 10.18 [5.09] μV, n = 6 animals; control amplitude = 5.45 [2.49] μV, n = 25 animals; P = 0.016), in cross-sectional comparisons, this was considered to result from inclusion of cats with relatively high predisease VEP amplitudes in this small group of 6 recovered cats (Fig. 2*F*). In some subjects with severe neurologic disease during active disease and progressive prolongation of VEP latency, the VEP waveform appeared broadened and flattened (Fig. 2*A*). In some cases this precluded identification of characteristic peaks and troughs of the feline VEP waveform and calculation of corresponding amplitudes and latencies.

ERGs and OCTs. Throughout the course of disease, no differences were identified in implicit time or amplitude of the A and B waves of

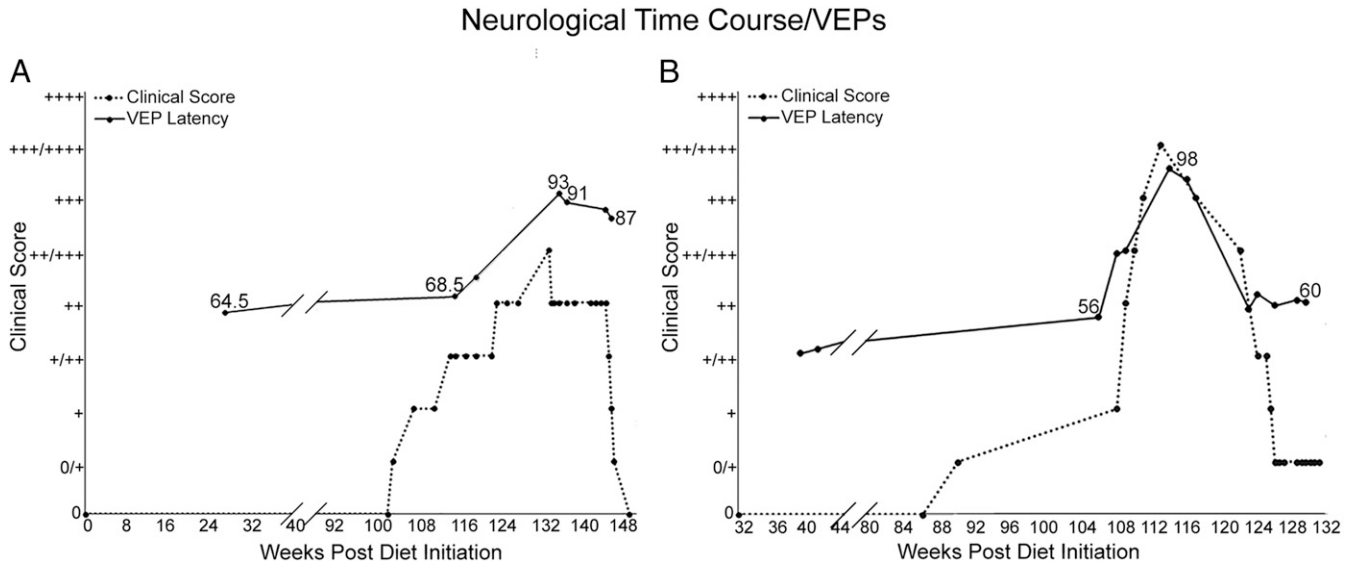

Fig. 1. Association between clinical course of the disease and VEP latency changes in FIDID. The severity of neurological signs, shown here in 2 cats, one moderately affected (*A*) and the second one with severe neurologic disease (*B*), is associated with prolonged VEP latency during acute disease, with subsequent shortening of latency as neurological signs abate. The neurological stages of disease were scored on a semiquantitative basis from 0 to 4+.

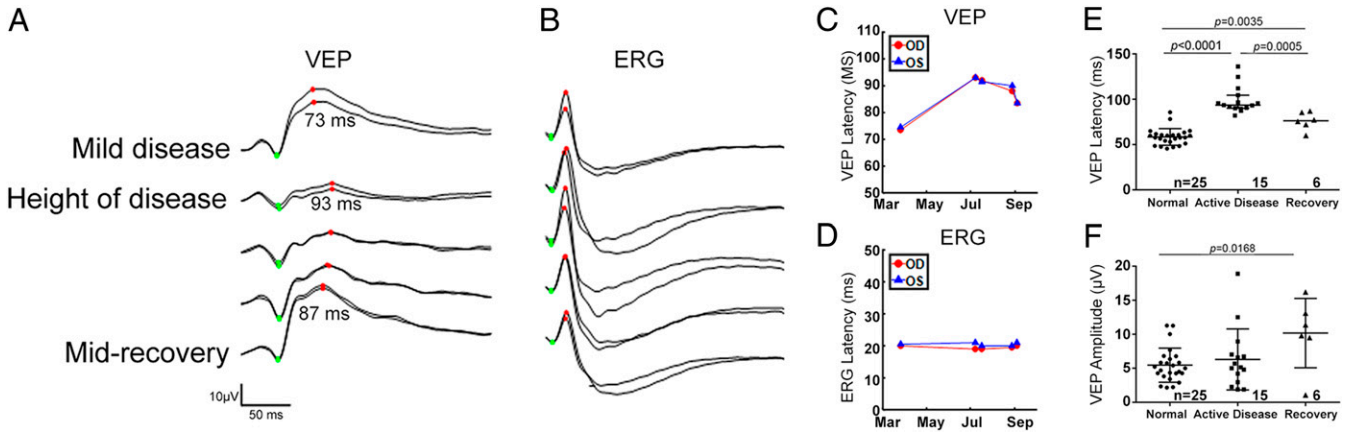

Fig. 2. VEP latency is significantly prolonged in cats with ON demyelination and recovers to near normal as remyelination proceeds. (*A*) Monocular photopic VEPs. Right and left eyes are overlaid, recorded simultaneously with the ERGs shown in *B* from the cat in Fig. 1*A*. Right- and left-hemisphere VEPs were combined before averaging 2 replications of 80 flash averages for each eye. The P2-like wave of the flash VEP is indicated by red dots. (*B*) Representative monocular photopic ERGs. Right and left eyes tracers are overlaid, and each trace is the average of two 80-flash averages. The stimulus was a 2.7-cd-s·m^{-2} white flash on a 30-cd·m^{-2} white background. Photopic ERG A and B waves are indicated by green and red dots, respectively. (*C*) Latency of the P2-like wave of the flash VEP shown in *A* increases during disease and shows partial return to pre-FIDID levels during recovery. (*D*) Latency of the photopic B waves shown in *B* is unchanged across the test intervals. (*E*) Mean latency of the P2 component of the feline flash VEP waveform (normal control mean [SD] = 58.46 [9.11] ms, $n = 25$; active disease = 98.88[14.76] ms, $n = 15$; recovery = 76.28 [9.85] ms, $n = 6$). (*F*) Mean amplitude of P2 component of the VEP is highly variable but not significantly impacted by active disease (normal control mean [SD] = 5.45 [2.49] μV, $n = 25$; active disease = 6.30 [4.48] μV, $n = 15$; recovery = 10.18 [5.09] μV, $n = 6$). Although amplitude was significantly higher in the small group of recovered cats than in control cats, this was attributed to high predisease VEP amplitudes in the former group in this cross-sectional comparison (horizontal black line, mean; error bars, SD; ANOVA with Tukey's multiple-comparisons posttest).

the photopic electroretinogram (ERG), with any observed differences between recording sessions falling within the range of intersession variability for control feline ERGs in our laboratory (Fig. 2 *B* and *D*). Optical coherence tomography (OCT) scans of the ON and retinal layers performed on 11 cats prior to disease onset and again during FIDID showed no evidence of loss of retinal nerve fiber layer thickness or other morphologic abnormalities within the retina (*SI Appendix*, Fig. S1).

Pathology of the ON during Active Disease. In 5 cats (minimal neurologic score ++), nearly all axons in the ONs were demyelinated or there was a mix of demyelination and remyelination indicating that practically all axons were demyelinated at some stage (Fig. 3 *C* and *D*). The extensive demyelination in active disease was in contrast to the recovered, remyelinated nerve (Fig. 3 *E* and *F*). To visualize the spatial distribution of demyelination/remyelination across and along the 5 levels of the ON from animals in active disease and recovered groups, images of serial sections of the ON were color coded with red and yellow dots representing remyelination and demyelination, respectively (Fig. 4 *A* and *B*). Both left and right ONs were affected similarly in each cat and myelin changes were seen along the entire length of each nerve. However, 2 trends were observed. First, the distal end of the nerve, closest to the chiasm (levels 1 and 2), was most severely demyelinated (Fig. 4*B*), especially the core of the nerve which contains a higher proportion of large-diameter axons. Second, remyelination, which occurred during active disease as it does in the spinal cord, was more extensive in the proximal nerve (levels 4 and 5) (Fig. 4 *C* and *F*). In addition, small- and medium-diameter axons of the subpia were preferentially remyelinated over those in the core (Fig. 4 *D* and *E*).

In cats euthanized within 4 to 6 wk of disease onset, the ONs contained many macrophages/microglia containing myelin debris and others that had foamy lipid droplet inclusions (Fig. 4 *C*–*E*). In cats euthanized at later time points, these foamy macrophages predominated with little myelin debris remaining, a pattern seen after myelin breakdown in MS and other demyelinating diseases (39). There was no evidence of T cell infiltration in the neuropil or perivascular cuffing.

Two cats, which had improved neurologically but not fully recovered and consequently were excluded from statistical analyses in the clinically recovered group, had persistently prolonged VEP latencies (~80 to 85 ms) but showed an unexpectedly high degree of remyelination of both ONs (Fig. 5*A*). In the first one (clinical score +++ to +), scattered demyelinated axons were seen in levels 1 and 2 (close to the chiasm) (Fig. 5 *B* and *C*) but few if any demyelinated axons or macrophages were seen in the more proximal levels 3 to 5 (closer to the retina) (Fig. 5 *D*–*G*). Examination of longitudinal sections from level 1 showed that there was a range in myelination along single axons, with frequent demyelinated segments and short remyelinated internodes (Fig. 6 *A*–*D*). Closer examination of the transverse sections of the ON showed that there was a gradient of thickness of the remyelinated axons with those close to the retina in levels 3 and 4 having thicker myelin than those in level 2 which is closer to the chiasm ($n = 2$ animals, g ratio at level 4 = 0.83, level 3 = 0.84, level 2 = 0.87; $P < 0.0001$) (see Fig. 8*C*). Indeed, many of the remyelinated axons in level 2 had 5 or fewer myelin lamellae (Fig. 6 *E* and *F*), less than that required for restoration of conduction (2). In contrast, such a gradient of myelin thickness was not seen in 3 recovered cats where all axons were remyelinated and VEP latencies considerably shortened although were prolonged relative to predisease values for these cats. In these cats ($n = 3$ animals) the mean g ratios at levels 2, 3, and 4 were 0.83, 0.84, and 0.83, respectively, confirming that remyelination was similar along the length of the nerve.

In the second partially recovered cat (clinical score +++ to ++), in each ON at level 2, the core of the nerve remained substantially demyelinated. We conclude that these 2 cats were examples of partial remyelination of the ON in which a significant number of demyelinated axons remained in addition to incomplete remyelination of many axons (g ratio = 0.86, <5 myelin lamellae). This incomplete remyelination led to improved yet still delayed VEP latencies relative to the reference population.

Pathology of the ON on Recovery. In marked contrast to the global demyelination seen when cats had a neurologic score of ++ or more, those that had recovered totally (0) or close to normal (+) showed complete or almost total remyelination (Figs. 3 *E* and *F*

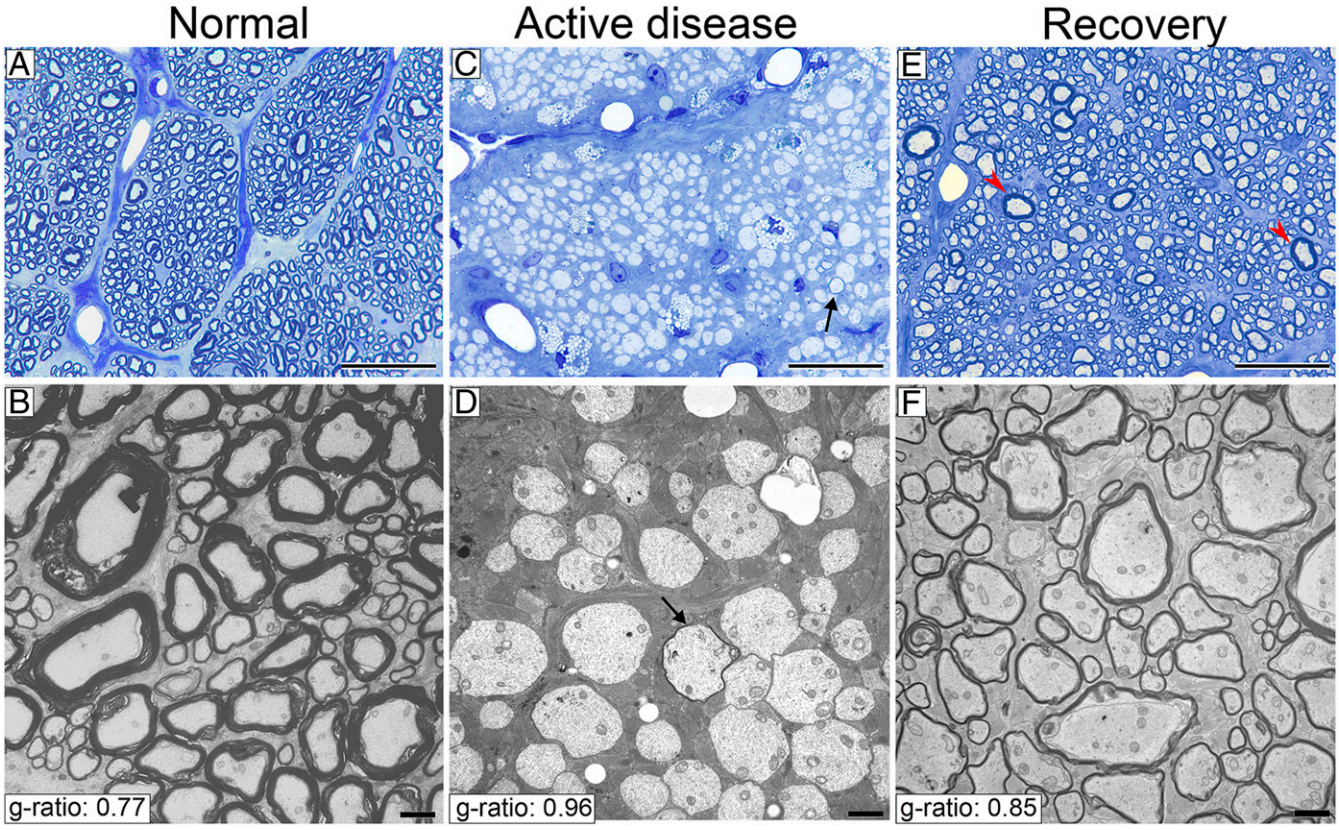

Fig. 3. Almost all ON axons were demyelinated during active disease and then remyelinated on return to normal diet in the recovery protocol. Light and electron microscopic images of the ON in control animals show normal thick myelin (*A* and *B*), complete demyelination of almost all axons in the ON of animals with active disease (*C* and *D*), rare axons are remyelinated (arrows in *C* and *D*), and complete remyelination after recovery (*E* and *F*). Rare axons with thick myelin are likely axons that were not demyelinated (*E*, red arrowheads). (Scale bars: *A*, *C*, and *E*, 20 μm; *B*, *D*, and *F*, 2 μm.)

and 4*B*). Quantitative scoring of the entire ON across the 5 levels showed a significant increase in the remyelination status along the nerve after recovery compared to the active disease group (active disease group $n = 5$, recovery group $n = 3$; $P = 0.0002$) (see Fig. 8*B*). Light microscopy showed that the majority of axons had thin myelin sheaths at all levels of both nerves, with only rare demyelinated and mature myelin sheaths present (Fig. 3*E*). Longitudinal sections of these nerves showed that thin myelin sheaths had short internodes (less than 100 μm) (Fig. 7 *A* and *B*). Foamy macrophages were seen to persist in the nerves, even though they were completely remyelinated.

Axons of all diameters were remyelinated with high g ratios (Fig. 7 *C* and *D*). The average g-ratio measurement across the entire ON from all clinically recovered animals confirmed the significant remyelination of all axons compared to control cats (recovered group g ratio = 0.85, $n = 6{,}733$ axons, $n = 3$ animals and control group g ratio = 0.77, $n = 3{,}157$ axons, $n = 3$ animals; $P < 0.0001$) (Figs. 3 *B* and *F* and 8*A*). Measurement of g ratios across the entire nerve confirmed the global remyelination (Fig. 4 *H* and *I*). The extent of demyelination and remyelination in the whole ON is illustrated in Movie S1 across the diameter of respective nerves.

While the predominant change seen during active disease and recovery was in the myelin sheath, i.e., demyelination and then subsequent remyelination, the question of the effect of the disease on axons is important. Only one cat, which had a long disease time course (1 y), displayed any apparent loss of axons, yet had subjectively intact vision. There was a progressive distal loss of axons in the core of the nerve but ~50% of axons remained at this level, which were predominately demyelinated. While no VEP was recordable in this subject, this is not surprising given the severe demyelination seen in levels 2 to 5. In the single cat that was judged to be clinically blind, vision loss was not attributable to axon loss but to extensive myelin vacuolation and global demyelination at levels 1 and 2 (right) or 4 (left) of the ONs (*SI Appendix*, Fig. S3). This cat had a clinical score of ++++ confirming the severe myelin changes in the spinal cord and brain. In the clinically recovered cats and the remainder of those in active disease, there was either no or very mild scattered axon loss (Fig. 4*B*).

While severely affected VEP waveforms for which the major positive peak could not be reliably identified were excluded from correlation analysis, VEP latency changes during active disease and after recovery were significantly correlated with changes in the remyelination status of the ON, confirming that VEP latency alteration is a valuable indicator of alteration in myelin thickness of the ON (active disease group $n = 2$, recovery group $n = 3$, $r = 0.937$; $P = 0.006$) (Fig. 8*D*).

Discussion

The results presented here definitively demonstrate a major increase in the VEP latency in the ONs of cats with FIDID during active disease followed by a progressive decrease in the latency during neurologic recovery. Histologic evaluation clearly showed that during active disease, practically all of the myelinated axons along the length of the nerve were demyelinated and then subsequently remyelinated following return to the recovery protocol. This model has systematically studied neuropathological evidence of the effects of remyelination on the VEP. Previously, the effect of demyelination on the VEP was evaluated after the injection of lysolecithin into the ON (19) or chiasm (20) or in EAE

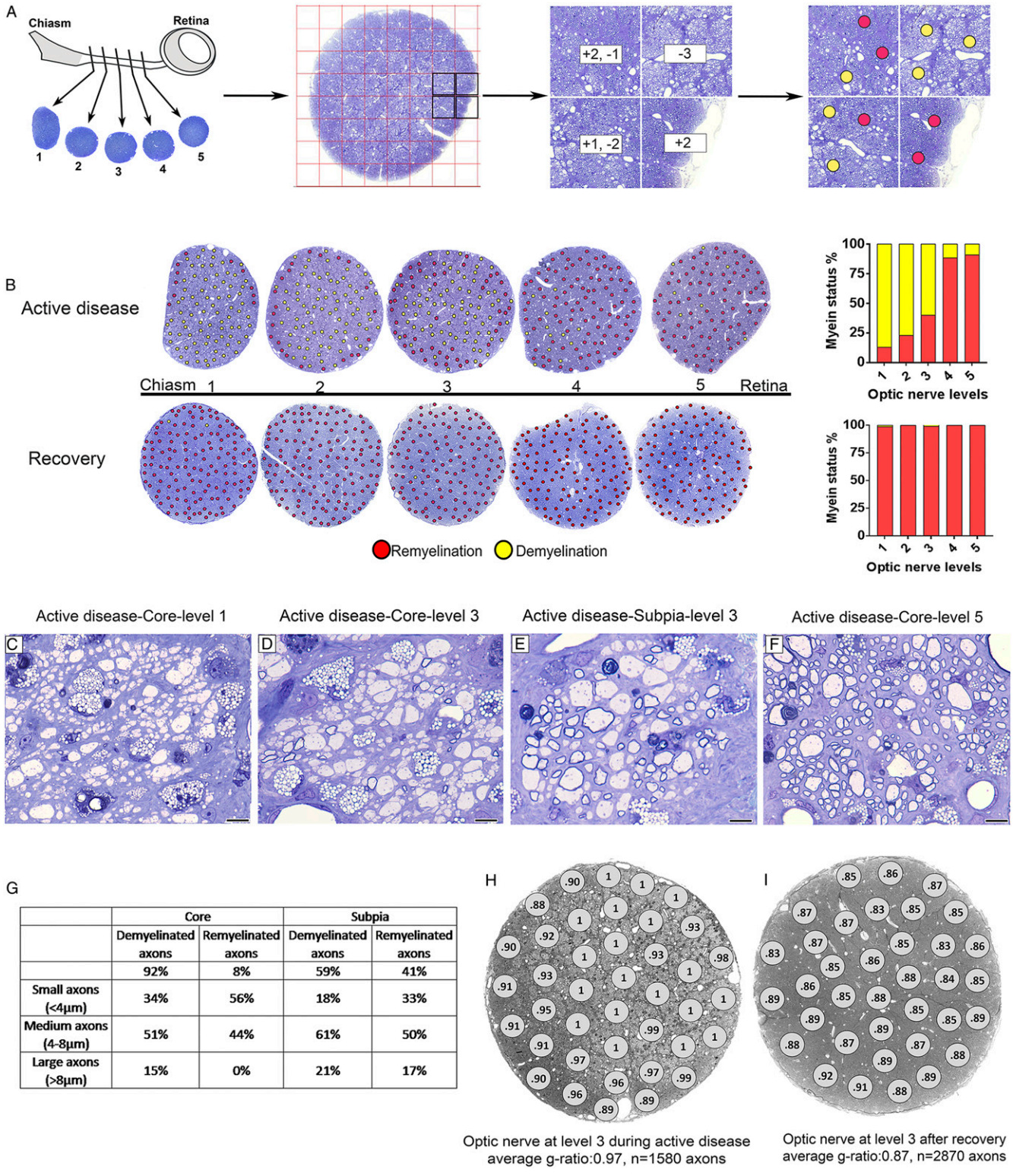

	Core		Subpia	
	Demyelinated axons	Remyelinated axons	Demyelinated axons	Remyelinated axons
	92%	8%	59%	41%
Small axons (<4μm)	34%	56%	18%	33%
Medium axons (4-8μm)	51%	44%	61%	50%
Large axons (>8μm)	15%	0%	21%	17%

Fig. 4. Spatial distribution of demyelination and remyelination in the ON during active disease and after recovery. (*A*) Schematic image of the ON: quantification and color coding strategy used to identify areas of demyelination and remyelination. Each ON was cut and labeled from 1 to 5 from the chiasm to retina. All areas of ON were scored for remyelination and demyelination and scores were replaced with red and yellow dots representing remyelination and demyelination, respectively. (*B*) Myelin status along the ON during active disease and after recovery showing distribution of demyelination and remyelination. In active disease, the ON is demyelinated in both the core and subpia, and then remyelination starts from subpia extending to the core at the retinal end of the nerve. On recovery, the entire nerve is fully remyelinated. Red and yellow dots represent remyelination and demyelination, respectively. (*C*–*F*) The majority of axons of all calibers are demyelinated in the core, proximal to the chiasm (levels 1 and 3), while small- and medium-caliber axons are the first axons remyelinated in the subpia. In contrast, most of the axons in the core proximal to the retina (level 5) are remyelinated. (*G*) Table shows the percentage of demyelinated and remyelinated axons of different sizes in *D* and *E*. (*H* and *I*) The ON at level 3 during active disease and after recovery showing g-ratio measurement in all areas across the ON. (Scale bar in *C*–*F*: 20 μm.)

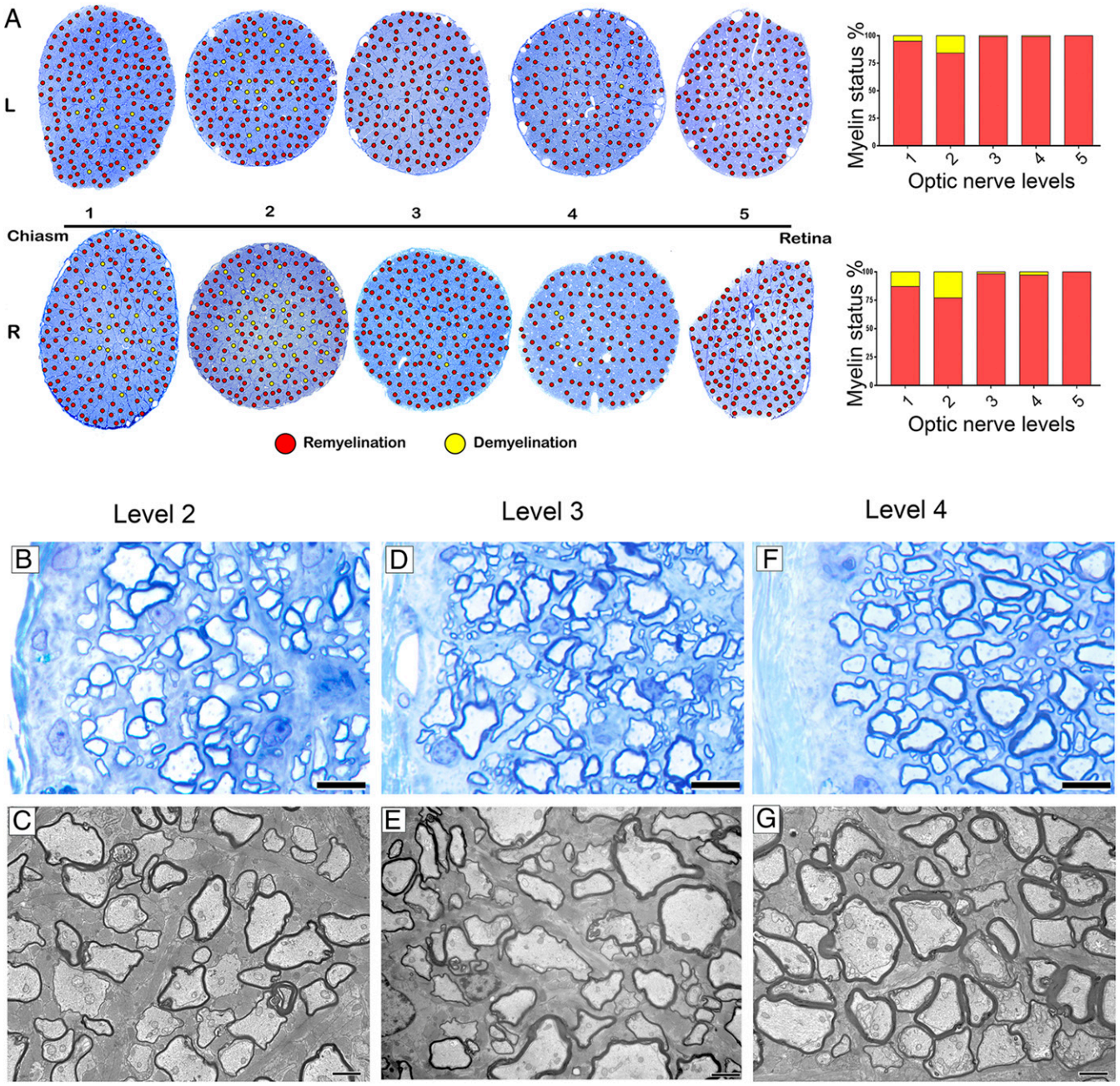

Fig. 5. Incomplete remyelination of the ON on partial neurologic recovery. (*A*) In one cat that had improved neurologically (+++ → ++) but had persistent, delayed VEP latencies, there was extensive remyelination along the lengths of both nerves. (*B*–*G*) However, the myelin sheath thickness of remyelinated axons appeared less in level 2 compared to levels 3 and 4 in both the subpia (*B*, *D*, and *F*) and the core (*C*, *E*, and *G*). (Scale bars: *B*, *D*, and *F*, 4 μm; *C*, *E*, and *G*, 2 μm.)

(40). However, in these models, a combination of pathologic changes including edema, inflammation, and axon loss were present that can confound interpretation of changes in the VEP. In a reductionist approach in FIDID, we asked whether the simple loss of myelin alone without these additional pathologic changes is sufficient to result in prolonged latencies of the VEP. Likewise, will remyelination in the presence of a normal complement of axons result in a subsequent decrease in latency of the VEP? The data presented here confirm that both hold true and that the VEP latency is a valid surrogate marker of demyelination and then remyelination of the ON.

As a compound response that depends upon the summation of potentials generated throughout the visual pathway, the scalp-recorded VEP is not just a measure of ON function but relies on functional and structural integrity of the retina (verified in our subjects by ERG and OCT), as well as central visual pathways, including optic tracts, optic radiations, and visual cortex. As with MS and optic neuritis, demyelination in FIDID also affects the brain (41). Lesions in higher visual pathways in demyelinating disease can alter the VEP to varying degrees (42). However, MRI and morphologic studies in recovered cats demonstrate axons are intact (41) and there is robust remyelination throughout the brain as in the ON. Here we show that the latency of the cortical VEP tracks well with the myelin status of the ON in FIDID, acknowledging there may be contributions from higher visual centers that are undergoing changes similar to those in the ON.

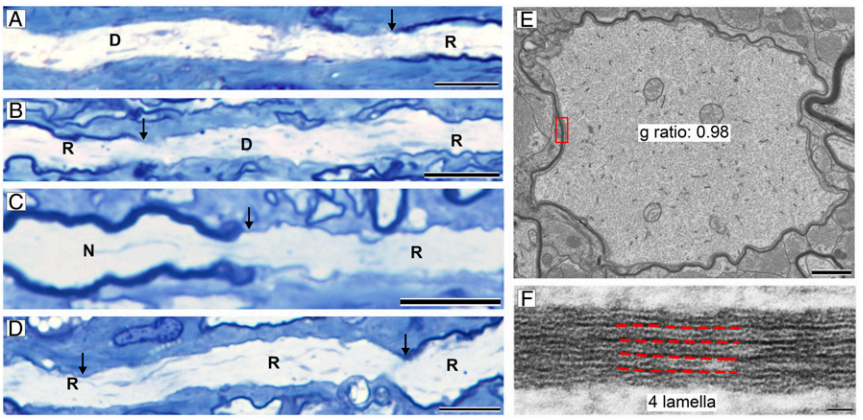

Fig. 6. Short internodes with thin myelin in partially recovered ONs. (*A–D*) Longitudinal sections at level 1 showed that many internodes were short and thin, demyelinated (D), remyelinated (R), or normal (N) (arrows mark nodes or heminodes). (*E*) EM examination of the ON at level 2 showed that many thinly myelinated axons had 5 or fewer myelin lamellae. (*F*) Boxed area from *E*. (Scale bars: *A–D*, 20 μm; *E*, 1 μm; and *F*, 20 nm.)

The pattern reversal VEP has been widely applied as a robust measure of ON function in patients with suspected optic neuritis since early studies (10, 43) identified consistent latency prolongation in patients with MS, even those with no clinical history of visual symptoms. In humans, pattern reversal VEP is considered more reproducible than the flash VEP. Flash VEP, as utilized in our study, is also considered less sensitive to dysfunction of the visual pathways than pattern VEP protocols in human patients, but is less affected by refractive error and opacity of ocular media and, most importantly in our animal studies, does not rely on reliable fixation of subjects on a pattern stimulus (44, 45). With extreme prolongation of VEP latency associated with longer duration, severe disease, the main VEP peak broadened substantially in several FIDID subjects, resulting in "flattening" of the waveform, which may have conceivably led to misidentification of smaller, unmasked peaks as P2 in these subjects. Thus, only VEPs acquired at time points during active disease at which P2 could be reliably identified were included in subsequent statistical comparisons between groups. This phenomenon of broadening of the VEP waveform, which may also be recognized in human patients with optic neuritis, contributed to an apparent reduction in VEP amplitude, inconsistently observed in some cats during active neurologic disease (46). However, this flattening of the VEP waveform peak in cats occurred in the absence of pronounced axon loss, as evidenced by histopathology, or subsequent recovery of normal VEP waveform and amplitude. In these subjects, we hypothesize that this waveform flattening effect results from a desynchronization of signals at the level of the cortex, produced by observed variable and nonuniform demyelination and remyelination in the context of relative preservation of ON axons. This is consistent with a similar hypothesis advanced by Urbach et al. (47) in their time domain analysis of flash VEP waveform abnormalities in MS. Preservation of axons in FIDID is particularly pertinent to MS, in which demyelination precedes axon loss [You et al. (42)]. Lack of thinning of the retinal nerve fiber layer (RNFL) on OCT up to 11 mo after disease development with normal ERGs excludes retinal abnormalities affecting the overall waveform of the VEP in subjects with active disease. Thus, changes in the VEP latency in FIDID reflect changes in myelin in the ON and not ganglion cell or axon loss in the retina.

We have previously shown that feeding an irradiated diet to cats results in generalized demyelination and subsequent remyelination in the brain, spinal cord, and ONs (5, 48, 49). In the present study we have delineated both qualitatively and quantitatively the extent of demyelination and remyelination along the length of both ONs in cats during active disease and recovery. In the 3 recovered cats (with clinical score 0), the ONs were completely remyelinated from retina to chiasm (g ratio 0.83 to 0.87) with only rare demyelinated axons present. Longitudinal sections of these nerves demonstrated that internodes were short, confirming the criteria for remyelination. We identified 2 cases in which ON remyelination was incomplete yet very different from the demyelinated nerve seen in active disease. In these nerves, close to the chiasm, scattered axons or groups of axons in the core of the nerve remained demyelinated, often associated with foamy macrophages. In addition, the g ratios in the distal segments of the nerve were higher than that at the proximal (retinal) end of the nerve. These findings suggest a gradient of remyelination. This spatial difference that we

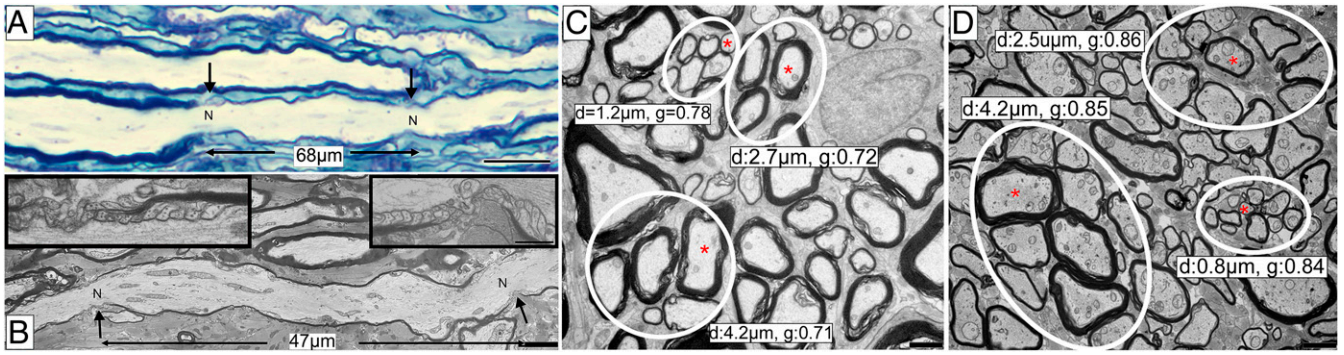

Fig. 7. Axons of all calibers in recovered animals were remyelinated with thin sheaths and short internodes. (*A*) A longitudinal section from the recovered animal shows a short, remyelinated internode between internodes with different myelin thickness (arrows mark nodes). (*B*) On EM, the short internode is demarcated by 2 nodes of Ranvier with paranodal loops (*Insets*). (*C*) Axon caliber and g ratios of small, medium, and large axons with normal myelin thickness in the control ON. (*D*) In the remyelinated nerve all axons of different calibers (small, medium, and large) had high g ratios, confirming remyelination. Red asterisks show axons with associated diameter and g ratio (*C* and *D*). N, node; d, diameter; g, g ratio. (Scale bars: *A*, 20 μm; *B–D*, 2 μm.)

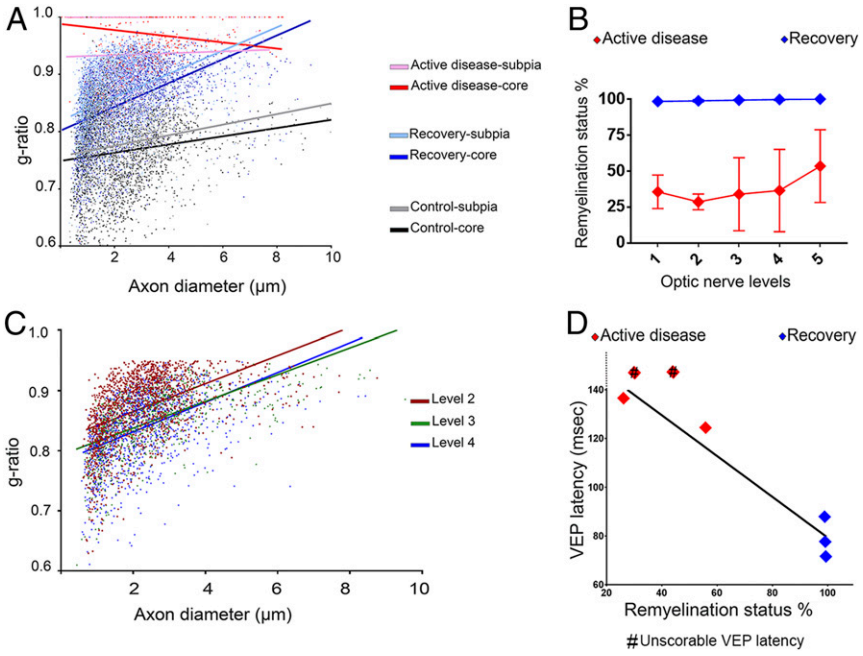

Fig. 8. Demyelination and remyelination of ON are significantly correlated with VEP latency. (*A*) Myelin thickness measurements show significant difference in the g ratio in the core and subpia of the ONs during active disease, after recovery, and in control (active disease, $n = 2$; recovery, $n = 3$; control, $n = 3$; $n \sim 11{,}500$ axons counted; multiple linear regression test, $P < 0.0001$). (*B*) Quantitative scoring of the myelin status shows a significant increase in remyelination along the ONs after recovery compared to ONs during active disease (active disease, $n = 5$; recovery, $n = 3$; 2-way ANOVA with Tukey's multiple-comparisons posttest, $P = 0.0002$). Error bars show SD. (*C*) A gradual change in the myelin thickness was seen from levels 2 to 4 in partially recovered animals ($n = 2$ animals, $n = 4{,}097$ axons counted, multiple linear regression test, $P < 0.0001$). (*D*) Myelin status of the ON and VEP latency are significantly correlated ($n = 5$; simple linear regression test, $r = 0.937$; $P = 0.006$). The VEPs latencies of 2 animals from the active disease group with low remyelination status were highly delayed but unscorable; these are marked by # in the plot but were excluded from statistical regression analysis.

believe results from the later onset of demyelination and then remyelination in the distal nerve is similar to that which occurs temporally, following lysolecithin lesion in the cat spinal cord, wherein at 3 mo after injection, remyelinated axon sheaths are thicker than at 2 mo (3). The lack of foamy macrophages and demyelination in the proximal nerve would also suggest that it was demyelinated before the distal segment, resulting in a temporal gradient of remyelination (39). It would appear that complete remyelination is essential for the shortening of VEP latencies to near-normal values.

The extent of the demyelination in the FIDID ON matches the size of large ON lesions in MS (16). As measured by MRI, lesions in optic neuritis had a length of 20 to 25 μm (50), similar in length to the cat ON, although the diameter of the human orbital ON is greater (4.5 to 5.0 mm compared to 1 to 2 mm in the cat). A single pathologic study of the extent of demyelination in MS in 18 patients with long-lasting disease has shown that the entire nerve can be demyelinated (16). Thus the demyelination seen in FIDID approximates large but partial lesions in human ONs.

What is the relevance of the data presented here to MS and future remyelination trials in which outcome measures are crucial? It might be assumed that imaging of the ON either by MRI or by positron emission tomography (PET) would be the optimal approach to measuring remyelination. However, the assessment of remyelination in vivo using noninvasive imaging methods is challenging—particularly in very small structures like the ONs (31). To date, no imaging measure of remyelination has satisfied the 5 prerequisites for use in clinical trials set forth by Barkhof et al. (51): pathological specificity, reproducibility, sensitivity to change, clinical relevance, and responsiveness to treatment. Conventional MRI is largely qualitative and, while unquestionably useful in the clinical setting, fails to distinguish remyelination from the myriad pathological changes that may coexist (e.g., inflammation, demyelination, axonal loss). Several, more quantitative MRI measures have shown significant correlations with myelin content but demonstrations of specificity have been elusive. There is potential for greater myelin specificity through PET ligands (e.g., [11C] MeDAS, [11C]CIC, [11C]PIB) that preferentially bind to myelin membrane constituents (52), although spatial resolution may be too limited for use in the ON. Studies in patients with MS and optic neuritis demonstrated increased radial diffusivity in the optic radiations to the visual cortex (42), suggesting that changes in central targets of the ON could play a role in altered VEPs in addition to ON demyelination.

Despite these limitations of existing imaging modalities, the ON remains the ideal structure in which to evaluate remyelination, as VEPs should be a reliable functional measure (26, 50, 53). Many studies have shown VEP latency increases in optic neuritis, a frequent presenting symptom in MS (10). Importantly, alteration of VEP latencies has been reported in 35% to 93% of patients that are clinically asymptomatic for visual system impairment (11, 46, 54–56). Thus, the ON provides an important and relevant clinical target in which to study and quantitate remyelination through VEP recordings. A number of studies have identified improvement in VEPs in patients being treated with disease-modifying therapies (57, 58). However, these observations were secondary to the primary outcome measures of these trials. In contrast, the VEP was the primary outcome measure in the RENEW (32) and ReBUILD (33) where the goal was to promote remyelination. The authors concluded in the first trial that the treatment with opicinumab did not show a shortening of latency at 24 wk. Although a significant reduction in VEP latency was observed in the per protocol group at week 32, this did not conclusively provide evidence of remyelination (32). Treatment with clemastine fumarate (ReBUILD trial) showed modest shortening of the VEP latency in both trial arms of the study and based on their previous animal model studies using this drug, the authors proposed that these results showed evidence of drug-promoted remyelination (33). Histologic evaluation of remyelination in the ONs was naturally impossible in these trials, and therefore it remains to be determined whether observed changes in the VEP latency truly reflect remyelination in human patients. Until now, the lack of an appropriate animal model in which demyelination and remyelination of the ON are robust has prevented this from being determined. In FIDID we were able to quantify the VEP throughout myelin loss and recovery and correlate latency and amplitude with the structural changes in the nerve.

We conclude that generalized demyelination during active disease leads to up to 2-fold prolongation of latency while in recovery, the VEP latency returns close to normal as a result of remyelination, if remyelination is complete. As thin myelin sheaths persist for extended periods (and likely indefinitely) (49), VEP latencies would not be expected to return to normal values as myelin remains thin

(3), yet is sufficient to allow normal ON function. During the recovery process, remyelination may be incomplete; i.e., some demyelination persists and myelin sheaths may be so thin (g ratio >0.95) that conduction remained slow, as we show here in 2 cats. Indeed, many axons in the distal segments of these cats had fewer than 5 lamellae and this would not support nerve conduction (2, 59). This incomplete remyelination could account for the persistence of delay in the VEP latency observed in some cats. It is likely that with longer follow-up, thin myelin sheaths will continue to accrue thicker myelin, accompanied by further reductions in VEP latency. The data presented here in a model characterized by ON demyelination and remyelination provide direct support to the suggestion that VEP recordings are true surrogate markers of remyelination (6, 26, 28, 30, 60) and will be a legitimate outcome measure in future clinical trials of remyelinating therapies in MS.

Materials and Methods

Animals. Sixteen female cats were fed an irradiated diet (45 to 55 kGy; Sterigenics Radiation Facility) for 5 to 18 mo, resulting in progressive neurological signs in 5 cats starting after 5 to 6 mo and following a more protracted course in 11 cats. Three control cats were fed a nonirradiated diet. Clinical signs resolved after return to a nonirradiated diet and daily s.c. vitamin B12 injections (0.5 mL SQ), which we refer to as the recovery protocol. While complete recovery can be achieved by return to feeding only nonirradiated food, we have previously found that adjunctive treatment with vitamin B12 may speed clinical neurological recovery (61). We therefore describe these combined changes in diet and B12 treatment as the recovery protocol. While the majority of cats had a similar temporal pattern of disease onset and course, a number of cats had a more protracted course during which initial ataxia/paresis resolved with later return to a progressive disorder requiring them to be maintained for up to 18 mo on irradiated food.

All cats were handled and treated in accordance with the Guide for the Care and Use of Laboratory Animals from the NIH, in compliance with protocols approved by Research Animal Resources Center and the Animal Care and Use Committee at the University of Wisconsin-Madison.

Clinical Evaluation. The neurologic course of disease was monitored by I.D.D. and by board-certified veterinary neurologists from the University of Wisconsin-Madison School of Veterinary Medicine. A semiquantitative scoring system was used to measure disease progression as follows: 0 = normal neurologic function, + = mild hind-limb (HL) ataxia, ++ = moderate HL ataxia, +++ = marked HL ataxia and paresis, ++++ = marked HL ataxia and severe paresis with some front limb abnormality. Cats with neurologic scoring of ++ to ++++ were considered at the "active disease" phase and returning to +/0 was considered as the "recovery" phase.

Two separate cohorts of cats were studied, with differences in overall study design but using the same protocols for recording and evaluating the VEP. In the first cohort, VEPs were recorded in 5 female cats at variable intervals, both before and after the development of neurologic disease. They were all around 1 to 1 1.5 y of age at the start of the irradiated diet. These cats were euthanized at varying intervals after the onset of neurologic signs and perfused as detailed below and both ONs collected. The second group of 11 female cats was studied in more detail, recording VEPs in 2 sessions, typically 7 to 8 d apart, at each time point to confirm reproducibility, predisease, during active disease and, in 6 of these 11n cats, during or following neurologic recovery (see below). These cats were perfused after complete recovery (score 0) or after a + or ++ improvement in neurologic function. Two were collected at the score of ++/+++ or +++.

Clinical assessment of ON function (direct and consensual pupillary light reflexes, menace responses, and dazzle reflexes) and subjective assessment of vision (visual placing reflexes and ability to track moving objects) were conducted by a board-certified veterinary ophthalmologist (G.J.M.).

Electrophysiological Recording. Cats were sedated with ketamine/xylazine and pupils were dilated with 0.5% tropicamide for each testing session. Pulse oximetry, rectal temperature, pulse rate and character, and respiratory rate were monitored throughout each procedure. The UTAS visual electrodiagnostic test system (LKC Technologies, Inc.) was used to acquire and store all electrophysiological responses as described below. A normative dataset, acquired as part of an unrelated study in the same laboratory, was available for statistical comparisons. These data were collected using an identical protocol for electrophysiological testing in 25 age-matched control cats.

Visual Evoked Potentials. Full-field (ff) transient flash VEP responses were recorded from subdermal needle electrodes overlying the right and left occipital cortices (62), approximating the location of the primary visual cortex (area 17), concurrent with ffERG as described below. Ganzfeld stimuli were 4.1-Hz white flashes delivered monocularly (2.7 cd-s·m^{-2} on a white 30-cd m^2 background), averaging 80 sweeps per trial, using a standard protocol for transient flash VEP recording with modification for cats (63). The cat flash VEP contains high-frequency wavelets, superimposed on the slow "P2" wave, which can make scoring problematic. To score these waveforms we used a low-pass filter to remove the high-frequency wavelets and simplify peak identification (*SI Appendix*, Fig. S4).

Flash ERG Recording. A single drop of 1% proparacaine solution was applied to each eye and a Barraquer eyelid speculum was inserted in both eyes. Gonak 2.5% Hypromellose solution was applied to the interior face of ERG-jet contact lens electrodes (Fabrinal) and electrodes were placed on the corneal surface of both eyes. Each contact lens electrode was referenced to a subdermal needle electrode inserted 2 cm from the ipsilateral lateral canthus. Ganzfeld stimuli were presented to light-adapted cats at intensities from 0.068 to 10.8 cd/m^2.

Waveform Analyses. Peak amplitude and time (latency) of the late positive component (P2) that characterizes the feline VEP waveform were measured using a custom software routine (MatlabR2018a; Mathworks). Root-mean-square (rms) of the early 0- to 35-ms portion of the VEP that contain the wavelets was calculated with custom software. Manual adjustments to the location of peak responses were made by an observer masked to the clinical status of the subjects. For ffERG analyses, A-wave and B-wave amplitudes and implicit times for each waveform were also automatically scored in Matlab, with manual correction of peak locations on the waveforms performed by a masked observer as necessary.

Optical Coherence Tomography. ON head (ONH) cube and raster scans were acquired in ketamine–xylazine anesthetized cats (n = 11) by spectral domain optical coherence tomography (sdOCT) and mean peripapillary RNFL thickness values derived by proprietary software (Cirrus version 6.0.2.81; Carl Zeiss Meditec Inc.) for 3 high-quality 200 × 200 ON cube scans for each eye.

Light and Electron Microscopy. Within 15 to 20 d of their final VEP recordings, animals were euthanized by pentobarbital sodium (120 mg/kg) and perfused with ice-cold PBS, followed by modified Karnovsky fixative. Both ONs (~2 cm in length) were removed and cut into segments labeled 1 to 5 from chiasm [1] to retina [5] (Fig. 4*A*). These segments were osmicated in 1% osmium tetroxide, dehydrated, and embedded in epoxy resin. Semithin (1-μm) sections from all 5 segments were stained with 1% toluidine blue and images were captured at 20× magnification using NIS-Elements v4.30 imaging software, a Nikon-Eclipse-E800 microscope, and a Nikon digital sight DS-Ri1 camera. Longitudinal sections from the same blocks were cut and stained. Ultrathin transverse and longitudinal and sections (<100 nm) were stained with uranyl acetate and lead citrate and electron micrographs were acquired with a Philips CM120 transmission electron microscope. Images were captured with a Software BioSprint 12 series digital camera using AMT Image Capture Software Engine V700.

Image Analysis. The remyelination and demyelination status in each toluidine blue-stained section was scored to determine the volume of each. A grid was placed over the image of the whole nerve and each window of the grid was scored from −1 to −3 showing demyelination (−3, complete demyelination) and +1 to +3 for remyelination (+3, complete remyelination). These were replaced with 1 to 3 yellow dots for demyelination and red dots for remyelination (Fig. 4*A*). Longitudinal sections were used for internode length measurement. Sections from the middle of the nerve (level 3) were used for electron microscopy imaging and quantitative analysis of the g ratio and axon diameter. Due to heterogeneity of demyelination and remyelination across the ON, electron micrograph images were taken from the center of each window of a 75-mesh grid, covering the entire area of the ON (*SI Appendix*, Fig. S2). The g ratio and axon diameters were measured for each ON using Fiji (ImageJ 1.51t) (64).

Statistics. VEP values were compared by one-way ANOVA and remyelination status was compared by 2-way ANOVA, both followed by Tukey's HSD test. Relationships between g ratio/axon diameters were tested by a multiple linear regression and between the VEP latency/remyelination by a simple linear regression. $P < 0.05$ denotes significance (statistical details in *SI Appendix*, Table S1).

Data Availability. All data relevant to this paper are available in the main text and *SI Appendix*.

ACKNOWLEDGMENTS. We acknowledge the assistance of Drs. C. B. Y. Kim, K. Snyder, and E. A. Hennes-Beean for assistance with acquisition of electrophysiological data; and C. A. Rasmussen for assistance with OCT scanning. We are grateful to Dr. I. Griffiths for his comments on the manuscript. This research was supported by the National Multiple Sclerosis Society (NMSS) Grant RG 1501-02876 (to I.D.D.) and The Myelin Project; NIH K08 EY018609 (to G.J.M.), R01 EY027396 (to G.J.M.), and Core Grant for Vision Research P30 EY016665; National Glaucoma Research Award G2016129 from BrightFocus Foundation (to G.J.M.); University of Wisconsin–Madison Office of the Vice Chancellor for Research and Graduate Education with funding from the Wisconsin Alumni Research Foundation (G.J.M.); and an unrestricted award to the University of Wisconsin–Madison Department of Ophthalmology and Visual Sciences from Research to Prevent Blindness.

1. R. J. M. Franklin, C. Ffrench-Constant, Regenerating CNS myelin–from mechanisms to experimental medicines. *Nat. Rev. Neurosci.* **18**, 753–769 (2017).
2. P. A. Felts, T. A. Baker, K. J. Smith, Conduction in segmentally demyelinated mammalian central axons. *J. Neurosci.* **17**, 7267–7277 (1997).
3. K. J. Smith, W. F. Blakemore, W. I. McDonald, The restoration of conduction by central remyelination. *Brain* **104**, 383–404 (1981).
4. N. D. Jeffery, W. F. Blakemore, Locomotor deficits induced by experimental spinal cord demyelination are abolished by spontaneous remyelination. *Brain* **120**, 27–37 (1997).
5. I. D. Duncan, A. Brower, Y. Kondo, J. F. Curlee, Jr, R. D. Schultz, Extensive remyelination of the CNS leads to functional recovery. *Proc. Natl. Acad. Sci. U.S.A.* **106**, 6832–6836 (2009).
6. G. Comi, L. Leocani, M. Onofrj, "Multiple sclerosis and other demyelinating disorders" in *Handbook of Clinical Neurophysiology*, G. G. Celesia, Ed. (Elsevier, 2005), vol. 5, pp. 491–516.
7. A. Compston *et al*., *McAlpine's Multiple Sclerosis* (Churchill Livingstone Elsevier, 2006), pp. 327–333.
8. A. Brusa, S. J. Jones, G. T. Plant, Long-term remyelination after optic neuritis: A 2-year visual evoked potential and psychophysical serial study. *Brain* **124**, 468–479 (2001).
9. S. J. Jones, A. Brusa, Neurophysiological evidence for long-term repair of MS lesions: Implications for axon protection. *J. Neurol. Sci.* **206**, 193–198 (2003).
10. A. M. Halliday, W. I. McDonald, J. Mushin, Delayed visual evoked response in optic neuritis. *Lancet* **1**, 982–985 (1972).
11. A. M. Halliday, W. I. McDonald, J. Mushin, Delayed pattern-evoked responses in optic neuritis in relation to visual acuity. *Trans. Ophthalmol. Soc. U. K.* **93**, 315–324 (1973).
12. G. Di Maggio *et al*., Optical coherence tomography and visual evoked potentials: Which is more sensitive in multiple sclerosis? *Mult. Scler.* **20**, 1342–1347 (2014).
13. G. Pihl-Jensen, M. F. Schmidt, J. L. Frederiksen, Multifocal visual evoked potentials in optic neuritis and multiple sclerosis: A review. *Clin. Neurophysiol.* **128**, 1234–1245 (2017).
14. D. Alshowaeir *et al*., Latency of multifocal visual evoked potentials in nonoptic neuritis eyes of multiple sclerosis patients associated with optic radiation lesions. *Invest. Ophthalmol. Vis. Sci.* **55**, 3758–3764 (2014).
15. C. Moll, C. Mourre, M. Lazdunski, J. Ulrich, Increase of sodium channels in demyelinated lesions of multiple sclerosis. *Brain Res.* **556**, 311–316 (1991).
16. J. Ulrich, W. Groebke-Lorenz, The optic nerve in multiple sclerosis: A morphological study with retrospective clinicopathological correlation. *Neurol Ophthalmol* **3**, 149–159 (1983).
17. A. R. Jennings, W. M. Carroll, Oligodendrocyte lineage cells in chronic demyelination of multiple sclerosis optic nerve. *Brain Pathol.* **25**, 517–530 (2015).
18. W. I. McDonald, T. A. Sears, The effects of experimental demyelination on conduction in the central nervous system. *Brain* **93**, 583–598 (1970).
19. Y. You, A. Klistorner, J. Thie, S. L. Graham, Latency delay of visual evoked potential is a real measurement of demyelination in a rat model of optic neuritis. *Invest. Ophthalmol. Vis. Sci.* **52**, 6911–6918 (2011).
20. S. Mozafari, M. A. Sherafat, M. Javan, J. Mirnajafi-Zadeh, T. Tiraihi, Visual evoked potentials and MBP gene expression imply endogenous myelin repair in adult rat optic nerve and chiasm following local lysolecithin induced demyelination. *Brain Res.* **1351**, 50–56 (2010).
21. W. M. Carroll, A. R. Jennings, F. L. Mastaglia, Galactocerebroside antiserum causes demyelination of cat optic nerve. *Brain Res.* **330**, 378–381 (1985).
22. W. M. Carroll, A. R. Jennings, F. L. Mastaglia, The origin of remyelinating oligodendrocytes in antiserum-mediated demyelinative optic neuropathy. *Brain* **113**, 953–973 (1990).
23. F. Lachapelle *et al*., Failure of remyelination in the nonhuman primate optic nerve. *Brain Pathol.* **15**, 198–207 (2005).
24. R. M. Ransohoff, Animal models of multiple sclerosis: The good, the bad and the bottom line. *Nat. Neurosci.* **15**, 1074–1077 (2012).
25. D. S. Reich, C. F. Lucchinetti, P. A. Calabresi, Multiple sclerosis. *N. Engl. J. Med.* **378**, 169–180 (2018).
26. L. J. Balcer, D. H. Miller, S. C. Reingold, J. A. Cohen, Vision and vision-related outcome measures in multiple sclerosis. *Brain* **138**, 11–27 (2015).
27. C. Tur *et al*., Assessing treatment outcomes in multiple sclerosis trials and in the clinical setting. *Nat. Rev. Neurol.* **14**, 75–93 (2018).
28. C. Barro *et al*., Fluid biomarker and electrophysiological outcome measures for progressive MS trials. *Mult. Scler.* **23**, 1600–1613 (2017).
29. M. Hardmeier, L. Leocani, P. Fuhr, A new role for evoked potentials in MS? Repurposing evoked potentials as biomarkers for clinical trials in MS. *Mult. Scler.* **23**, 1309–1319 (2017).
30. M. P. Sormani, M. Pardini, Assessing repair in multiple sclerosis: Outcomes for phase II clinical trials. *Neurotherapeutics* **14**, 924–933 (2017).
31. S. Mallik, R. S. Samson, C. A. Wheeler-Kingshott, D. H. Miller, Imaging outcomes for trials of remyelination in multiple sclerosis. *J. Neurol. Neurosurg. Psychiatry* **85**, 1396–1404 (2014).
32. D. Cadavid *et al*.; RENEW Study Investigators, Safety and efficacy of opicinumab in acute optic neuritis (RENEW): A randomised, placebo-controlled, phase 2 trial. *Lancet Neurol.* **16**, 189–199 (2017).
33. A. J. Green *et al*., Clemastine fumarate as a remyelinating therapy for multiple sclerosis (ReBUILD): A randomised, controlled, double-blind, crossover trial. *Lancet* **390**, 2481–2489 (2017).
34. J. P. Cassidy *et al*., Leukoencephalomyelopathy in specific pathogen-free cats. *Vet. Pathol.* **44**, 912–916 (2007).
35. G. Child, D. J. Foster, B. J. Fougere, J. M. Milan, M. Rozmanec, Ataxia and paralysis in cats in Australia associated with exposure to an imported gamma-irradiated commercial dry pet food. *Aust. Vet. J.* **87**, 349–351 (2009).
36. T. S. G. A. M. van den Ingh, G. C. M. Grinwis, R. J. Corbee, Leukoencephalomyelopathy in cats linked to abnormal fatty acid composition of the white matter of the spinal cord and of irradiated dry cat food. *J. Anim. Physiol. Anim. Nutr. (Berl.)* **103**, 1556–1563 (2019).
37. D. Creel, R. E. Dustman, E. C. Beck, Intensity of flash illumination and the visually evoked potential of rats, Guinea pigs and cats. *Vision Res.* **14**, 725–729 (1974).
38. J. Stone, The naso-temporal division of the cat's retina. *J. Comp. Neurol.* **126**, 585–600 (1966).
39. L. A. Boven *et al*., Myelin-laden macrophages are anti-inflammatory, consistent with foam cells in multiple sclerosis. *Brain* **129**, 517–526 (2006).
40. R. Diem *et al*., Autoimmune optic neuritis in the common marmoset monkey: Comparison of visual evoked potentials with MRI and histopathology. *Invest. Ophthalmol. Vis. Sci.* **49**, 3707–3714 (2008).
41. A. S. Field, A. Samsonov, A. L. Alexander, P. Mossahebi, I. D. Duncan, Conventional and quantitative MRI in a novel feline model of demyelination and endogenous remyelination. *J. Magn. Reson. Imaging* **49**, 1304–1311 (2019).
42. Y. You *et al*., Demyelination precedes axonal loss in the transneuronal spread of human neurodegenerative disease. *Brain* **142**, 426–442 (2019).
43. A. M. Halliday, W. I. McDonald, J. Mushin, Visual evoked response in diagnosis of multiple sclerosis. *BMJ* **4**, 661–664 (1973).
44. G. E. Holder, G. G. Celesia, Y. Miyake, S. Tobimatsu, R. G. Weleber; International Federation of Clinical Neurophysiology, International Federation of Clinical Neurophysiology: Recommendations for visual system testing. *Clin. Neurophysiol.* **121**, 1393–1409 (2010).
45. American Clinical Neurophysiology Society, Guideline 9B: Guidelines on visual evoked potentials. *J. Clin. Neurophysiol.* **23**, 138–156 (2006).
46. F. Shahrokhi, K. H. Chiappa, R. R. Young, Pattern shift visual evoked responses. Two hundred patients with optic neuritis and/or multiple sclerosis. *Arch. Neurol.* **35**, 65–71 (1978).
47. D. Urbach, M. Gur, H. Pratt, R. Peled, Time domain analysis of VEPs. Detection of waveform abnormalities in multiple sclerosis. *Invest. Ophthalmol. Vis. Sci.* **27**, 1379–1384 (1986).
48. I. D. Duncan *et al*., The adult oligodendrocyte can participate in remyelination. *Proc. Natl. Acad. Sci. U.S.A.* **115**, E11807–E11816 (2018).
49. I. D. Duncan, R. L. Marik, A. T. Broman, M. Heidari, Thin myelin sheaths as the hallmark of remyelination persist over time and preserve axon function. *Proc. Natl. Acad. Sci. U.S.A.* **114**, E9685–E9691 (2017).
50. A. Klistorner *et al*., Remyelination of optic nerve lesions: Spatial and temporal factors. *Mult. Scler.* **16**, 786–795 (2010).
51. F. Barkhof, P. A. Calabresi, D. H. Miller, S. C. Reingold, Imaging outcomes for neuroprotection and repair in multiple sclerosis trials. *Nat. Rev. Neurol.* **5**, 256–266 (2009).
52. B. Bodini *et al*., Dynamic imaging of individual remyelination profiles in multiple sclerosis. *Ann. Neurol.* **79**, 726–738 (2016).
53. A. Compston, Remyelination in multiple sclerosis: A challenge for therapy. The 1996 European Charcot Foundation Lecture. *Mult. Scler.* **3**, 51–70 (1997).
54. A. Tartaglione *et al*., Electrophysiological detection of "silent" plaques in the optic pathways. *Acta Neurol. Scand.* **76**, 246–250 (1987).
55. E. A. Sanders, J. P. Reulen, L. A. Hogenhuis, E. A. van der Velde, Electrophysiological disorders in multiple sclerosis and optic neuritis. *Can. J. Neurol. Sci.* **12**, 308–313 (1985).
56. D. Sisto *et al*., Subclinical visual involvement in multiple sclerosis: A study by MRI, VEPs, frequency-doubling perimetry, standard perimetry, and contrast sensitivity. *Invest. Ophthalmol. Vis. Sci.* **46**, 1264–1268 (2005).
57. A. Tsakiri *et al*., Simvastatin improves final visual outcome in acute optic neuritis: A randomized study. *Mult. Scler.* **18**, 72–81 (2012).
58. R. Iodice *et al*., Multimodal evoked potentials follow up in multiple sclerosis patients under fingolimod therapy. *J. Neurol. Sci.* **365**, 143–146 (2016).
59. Z. J. Koles, M. Rasminsky, A computer simulation of conduction in demyelinated nerve fibres. *J. Physiol.* **227**, 351–364 (1972).
60. A. Niklas, H. Sebraoui, E. Hess, A. Wagner, F. Then Bergh, Outcome measures for trials of remyelinating agents in multiple sclerosis: Retrospective longitudinal analysis of visual evoked potential latency. *Mult. Scler.* **15**, 68–74 (2009).
61. M. Heidari *et al*., Remyelination in the optic nerve detected by visual evoked potentials in a large animal model of demyelination. https://www.abstractsonline.com/pp8/#!/4649/presentation/23657. Accessed 20 February 2019.
62. L. B. Padnick, R. A. Linsenmeier, Properties of the flash visual evoked potential recorded in the cat primary visual cortex. *Vision Res.* **39**, 2833–2840 (1999).
63. J. V. Odom *et al*.; International Society for Clinical Electrophysiology of Vision, ISCEV standard for clinical visual evoked potentials: (2016 update). *Doc. Ophthalmol.* **133**, 1–9 (2016).
64. J. Schindelin *et al*., Fiji: An open-source platform for biological-image analysis. *Nat. Methods* **9**, 676–682 (2012).